energies

MDPI

Article

Geometry, Mesh and Numerical Scheme Influencing the Simulation of a Pelton Jet with the OpenFOAM Toolbox

Jean Decaix [1,*] and Cécile Münch-Alligné [2]

[1] Institute of Sustainable Energy, School of Engineering, HES-SO Valais-Wallis, Rue de l'Industrie 23, 1950 Sion, Switzerland
[2] Institute of Systems Engineering, School of Engineering, HES-SO Valais-Wallis, Rue de l'Industrie 23, 1950 Sion, Switzerland
* Correspondence: jean.decaix@hevs.ch

Abstract: Hydropower is a key source of electricity production for allowing the integration of intermittent renewable energy resources. Among the various hydraulic power plants around the world, the ones equipped with Pelton turbines already provide large flexibility that is still enhanced with the development, for instance, of the hydraulic short circuit operating mode. However, the knowledge of the flow inside Pelton turbines is still a challenging task, both numerically and experimentally, despite progress in the last two decades. One key feature of the Pelton efficiency is the jet quality, i.e., the jet velocity needs to be uniform, not perturbed by secondary flows and compact. The compactness of the jet is mainly dependent o nthe location of the jet detachment at the nozzle outlet, which is challenging for computational fluid dynamics simulations mainly due to numerical diffusion. Even if this point has already been mentioned in previous papers, the present paper focuses on all the parameters that can influence the jet detachment: the nozzle geometry, the mesh and the numerical scheme used to discretize the convective fluxes. The simulations of an existing Pelton injector are performed using the OpenFOAM toolbox. It is noticed that, in addition to the nozzle geometry and the mesh resolution at the nozzle outlet, the choice of the numerical schemes influences the jet detachment and, consequently, the jet diameter and discharge. The use of an anti-diffusive scheme such as the "SUPERBEE" limiter improves the prediction of the jet in accordance with the on-site measurements.

Keywords: CFD; Pelton turbine; jet; SUPERBEE; OpenFOAM

Citation: Decaix, J.; Münch-Alligné, C. Geometry, Mesh and Numerical Scheme Influencing the Simulation of a Pelton Jet with the OpenFOAM Toolbox. *Energies* **2022**, *15*, 7451. https://doi.org/10.3390/en15197451

Academic Editor: Galih Bangga

Received: 19 September 2022
Accepted: 7 October 2022
Published: 10 October 2022

1. Introduction

Hydropower is a key source of electricity production for offering an efficient integration of green variable generation sources of energy, such as solar and wind [1]. Among the various hydraulic turbines, the Pelton turbine has the advantage of keeping an efficiency higher than 80% over a discharge range from 20% to 120% of the nominal value [2]. Consequently, power plants equipped with such turbines are well suited to provide flexibility that can be improved by considering the headrace tunnel as an additional storage capacity [3,4]. Furthermore, pumped-storage power plants equipped with Pelton turbines have been designed in the last few years, such as the FMHL+ power plant [5] or the Grand'Maison power plant [6], to operate in hydraulic short circuit mode, allowing load-frequency regulation [7].

This development of new uses for Pelton turbines is accompanied by challenges in Pelton research that were underlined twenty years ago in the paper by Sick et al. [8]. Computational fluid dynamics (CFD) has provided valuable insights into the flow in Pelton turbines. However, the simulation of a Pelton runner is still a challenging task [9], even if new mesh-free solvers have been developed and used [10–13]. Another challenge for Pelton turbines, not considered in this paper, is the assessment of erosion in the Pelton injector due to solid particles. A solver coupling approach is often used to solve such a flow since the fluid is modelled based on eulerian modelling, whereas a Lagrangian framework is

used to solve the particle trajectories [14,15]. The hydro-abrasive erosion is then estimated using specific models than can deal with specific coating.

For Pelton turbines, a high-quality jet is required to reach an efficiency of at least 92% [16]. In this paper, the authors considered that jet quality is characterised by the uniform velocity distribution inside the jet, the absence of secondary flows and the compactness of the jet. Santolin et al. [17] compared an ideal jet with a real jet, showing the importance of the jet quality on the turbine efficiency, which decreases by two per cent compared to the real jet. The compactness of the jet is strongly dependent on the separation point of the jet at the nozzle outlet, as underlined by Mack et al. [18], who show the importance of locally refining the mesh at the outer diameter of the nozzle outlet to accurately predict the jet diameter. Indeed, in the absence of the mesh refinement, the water flow detaches downstream of the experimental one, and the jet diameter is overestimated. Jost et al. [19] used an automatic mesh refinement procedure to refine the mesh in regions where the gradients of water and air volume fraction are the largest. This procedure allows the prediction of the jet diameter with an accuracy of around 2% compared to the theoretical value. Fiereder et al. [20] also computed a Pelton jet and mentioned in the numerical setup that various high-order convection schemes can be used, such as the "MINMOD", "SMART", "OSHER" and "VANLEER". Unfortunately, they did not provide which scheme was used to achieve the results shown.

The role of the numerical scheme is not discussed in papers most of the time. One reason could be the use of the ANSYS CFX software by several authors [17,19] since only one high-resolution convective scheme based on the work of Barth et al. [21] is available. However, on the same mesh, the use of a low-diffusive scheme should impact the compactness of the jet compared to a higher-diffusive scheme. Therefore, it should be possible to achieve an accurate jet detachment with a coarser mesh, which can reduce the Computational Power Unit (CPU) needed for a simulation and relax the requirements on the Courant–Friedrichs–Lewy (CFL) number.

The present paper aims to focus on the parameters that influence the prediction of the jet detachment at the outlet of a Pelton injector. The parameters considered are the nozzle geometry, the mesh resolution and the limiter used for the discretisation of the convective fluxes. The test case considered is an existing Pelton injector installed at the power plant of Gletsch–Oberwald (KWGO) owned by the Forces Motrices Valaisannes (FMV) and investigated during the SmallFlex project [4]. Thanks to the field measurements, the discharge predicted by the simulation are compared with the measured one.

2. Modelling

To compute the Pelton jet, the homogeneous mixture Reynolds-Averaged Navier–Stokes (RANS) equations are considered [22], assuming a mechanical equilibrium between the fluids, which means that the two fluids (air and water) share the same velocity and the same pressure. In addition, the two fluids are assumed incompressible and immiscible. The set of RANS equations closed using an eddy viscosity assumption written in Cartesian coordinates:

$$\frac{\partial u_j}{\partial x_j} = 0 \tag{1}$$

$$\frac{\partial u_i}{\partial t} + \frac{\partial u_i u_j}{\partial x_j} = -\frac{1}{\rho}\frac{\partial p}{\partial x_i} + g + \frac{1}{\rho}F_s + (\nu + \nu_t)\frac{\partial^2 u_j}{\partial x_i \partial x_j} \tag{2}$$

with:

- u_i being the averaged mixture velocity vector.
- p being the averaged mixture pressure.
- ρ being the averaged mixture density computed as $\rho = \alpha\rho_{water} + (1-\alpha)\rho_{air}$.
- g being the gravity acceleration.

- F_s being the surface tension computed as $F_s = \sigma\kappa n$ with σ the surface tension (assumes constant), κ the local curvature of the interface and n the unit vector normal to the interface.
- ν being the mixture kinematic viscosity computed as $\nu = \alpha\nu_{water} + (1-\alpha)\nu_{air}$.
- ν_t being the eddy viscosity computed using the SST $k-\omega$ model [23] that solves two additional transport equations for the turbulent kinetic energy k and the turbulent frequency ω.
- α being the water volume fraction.

An additional transport equation for the liquid volume fraction α is required to close the system.

$$\frac{\partial \alpha}{\partial t} + u_j \frac{\partial \alpha}{\partial x_j} = 0 \tag{3}$$

Such a model is implemented in the *interfoam* solver available in the OpenFOAM toolbox [24] with a specific treatment for the transport Equation (3), which is rewritten as:

$$\frac{\partial \alpha}{\partial t} + \frac{\partial \alpha u_j}{\partial x_j} + \frac{\partial \left(\alpha(1-\alpha)u_{c,j}\right)}{\partial x_j} = 0 \tag{4}$$

with u_c as a suitable velocity to compress the interface, computed as:

$$u_c = \min(c_\alpha |u|, \max|u|) \frac{\nabla \alpha}{|\nabla \alpha|} \tag{5}$$

c_α is a user parameter set to its default value equal to 1 for the present study. For a more detailed explanation of the solver, the reader can refer to [25], in which the compression of the interface is formulated in terms of interface fluxes.

3. Geometry and Computational Domain

The Pelton turbine considered for the present study is a prototype setup in the power plant of Gletsch–Oberwald (KWGO) in Switzerland owned by FMV. The nominal power, head and discharge of the turbine are 7.5 MW, 287 m and 5.9 $m^3\ s^{-1}$, respectively. The unit features 6 jets and 21 buckets.

Two geometries of the nozzle are shown in Figure 1, one refers to the original geometry, and the second refers to a modified geometry without the flat section (red circle on the figure). The outer diameter of the nozzle outlet D_{Nozzle} is kept constant between the two geometries. Two needle strokes S will be considered in the study: S = 50%, which corresponds to the nominal stroke, and S = 85%, which is close to the maximum stroke opening in the normal operation of the turbine. Point O corresponds to the close position of the needle, i.e., $S = 0\%$.

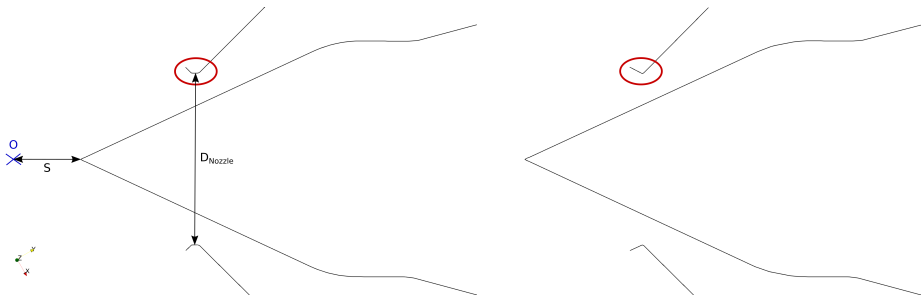

Figure 1. (**Left**): original geometry of the nozzle. (**Right**): modified geometry of the nozzle.

A half-view of the computational domain is shown in Figure 2. Only one injector is considered. An additional artificial volume is added downstream of the nozzle, allowing the development of the jet. The size of this volume is chosen in such a way that the six injectors can be computed if the whole Pelton manifold is considered.

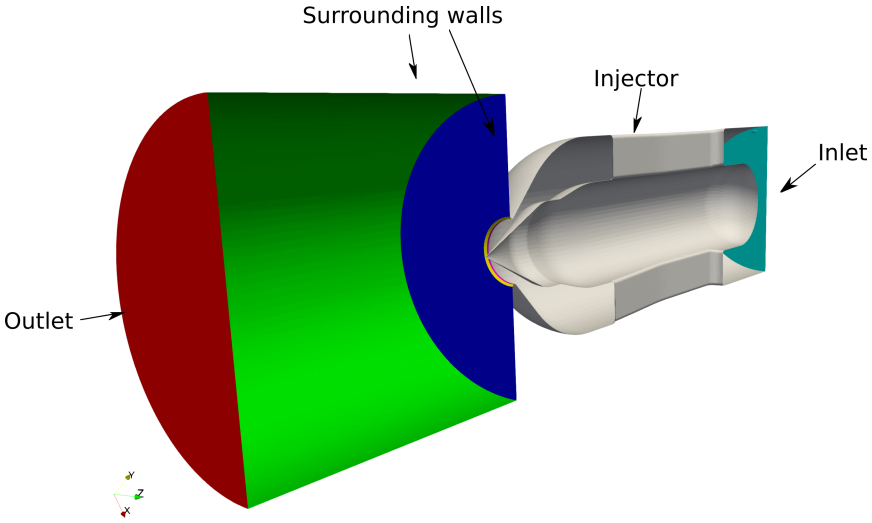

Figure 2. Half-view of the computational domain.

4. Mesh

Meshes are generated using the native mesher *snappyHexMesh* available with the OpenFOAM toolbox. This mesher allows the generation of a dominant Cartesian mesh based on a background mesh generated with the *blockMesh* utility. Overall, four meshes have been used: two meshes for a stroke of 50% with the original geometry, one for a stroke of 50% with the modified geometry and one for a stroke of 85% with the original geometry. Table 1 gives the number of points, cells and boundary cell layers for each mesh, whereas Table 2 gives the values of the mesh quality criteria: the maximum non-orthogonality, the skewness and the aspect ratio.

Table 1. Number of points, cells and boundary cell layers for each mesh.

Mesh	Geometry	Stroke (%)	Number of Points	Number of Cells	Number of Wall Cell Layers
1	Original	50	5.8×10^6	5.1×10^6	3
2	Original	50	10.1×10^6	9.3×10^6	3
1	Modified	50	5.8×10^6	5.1×10^6	3
1	Original	85	6.3×10^6	5.5×10^6	3

Table 2. Values of some mesh quality criteria.

Mesh	Geometry	Stroke (%)	Maximum Non-Orthogonality (deg)	Maximum Skewness	Maximum Aspect Ratio
1	Original	50	69	4.9	25
2	Original	50	70	4.9	25
1	Modified	50	69	6.7	26
1	Original	85	70	4.9	25

Beyond the number of cells, the difference between meshes 1 and 2 is how the background Cartesian mesh has been generated. For mesh 1, the background mesh is aligned with the axis of the nozzle, whereas for mesh 2, the background mesh is aligned with the local slope of the needle (see Figure 3).

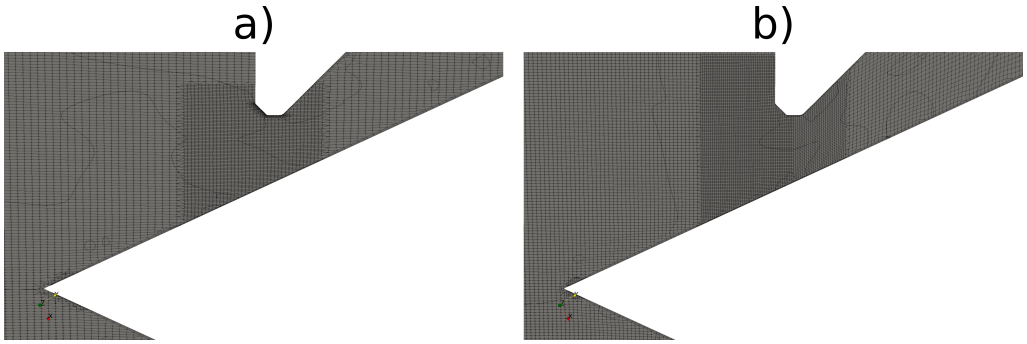

Figure 3. View of the mesh at the nozzle outlet. (**a**) Mesh 1 for the original geometry and a stroke S = 50%. (**b**) Mesh 2 for the original geometry and a stroke S = 50%.

Three cell layers are added close to the wall to accurately capture the boundary layer. The average y^+ value along the walls of the injector is around 60 for mesh 1 and 40 for mesh 2, which is in accordance with the use of a wall law for the turbulence model [26].

5. Numerical Setup

Equation (4) is solved first using the Flux-Corrected Transport (FCT) method described in [27] and the method called Multidimensional Universal Limiter for Explicit Solution (MULES) in OpenFOAM. Then, the pressure–velocity coupling is solved using the PIMPLE algorithm, which is a mixture of the SIMPLE and PISO algorithms. For the present study, the velocity prediction is skipped, i.e., the "momentum Predictor" entry in the "fvSolution" file is set to "no". Therefore, the velocity is updated only after solving the pressure equation. Two loops over the pressure equation are carried out (i.e., the "nCorrectors" entry is set to 2 in the "fvSolution" file) with, in addition, two loops for the non-orthogonal corrections of the fluxes (i.e., the "nNonOrthogonalCorrectors" entry is set to 2 in the "fvSolution" file). An implicit Euler scheme is used for the pseudo-time marching advancement of the solution with a pseudo-time step set to 10^{-3} s with, in addition, under-relaxation coefficients for the conservative equations (their values are discussed in Section 6).

The convective fluxes of the momentum equation are discretized using a high-resolution (HR) scheme based on the Total Variation Diminishing (TVD) framework [28]. The "limitedLinear" and the "SUPERBEE" limiters are considered in the present study (see Equations (6) and (7)). The "limitedLinear" limiter is more diffusive than the "SUPERBEE" limiter, since, in the Sweby diagram (see Figure 4), the "SUPERBEE" limiter matches the downwind scheme, which is characterized by a negative truncation error responsible for an additional anti-diffusive component in the equation to be solved. On the contrary, the upwind scheme has a positive truncation error associated with diffusive behaviour. Therefore, a limiter is diffusive if it is closer to the upwind scheme in the Sweby diagram and anti-diffusive otherwise. The convective fluxes of the SST turbulent model are discretized using an upwind scheme.

$$\text{limitedLinear} \quad \Psi(r) = \max(\min(2r, 1), 0) \tag{6}$$

$$\text{SUPERBEE} \quad \Psi(r) = \max(\max(\min(2r, 1), \min(r, 2)), 0) \tag{7}$$

where $\Psi(r)$ is the limiter applied to the numerical scheme, and r is computed as the ratio of two consecutive gradients (for more details, the reader can refer to the book of Moukalled et al. [28]).

The total pressure is set at the inlet boundary to match the nominal head of the power plant. At the outlet, a fixed mean static pressure is imposed with a value of 1 bar, and no backflow is permitted (this setup improves the initialisation of the jet development). The solid walls of the injector are considered no-slip walls, whereas the side walls of the artificial volume downstream of the nozzle are considered as free slip walls.

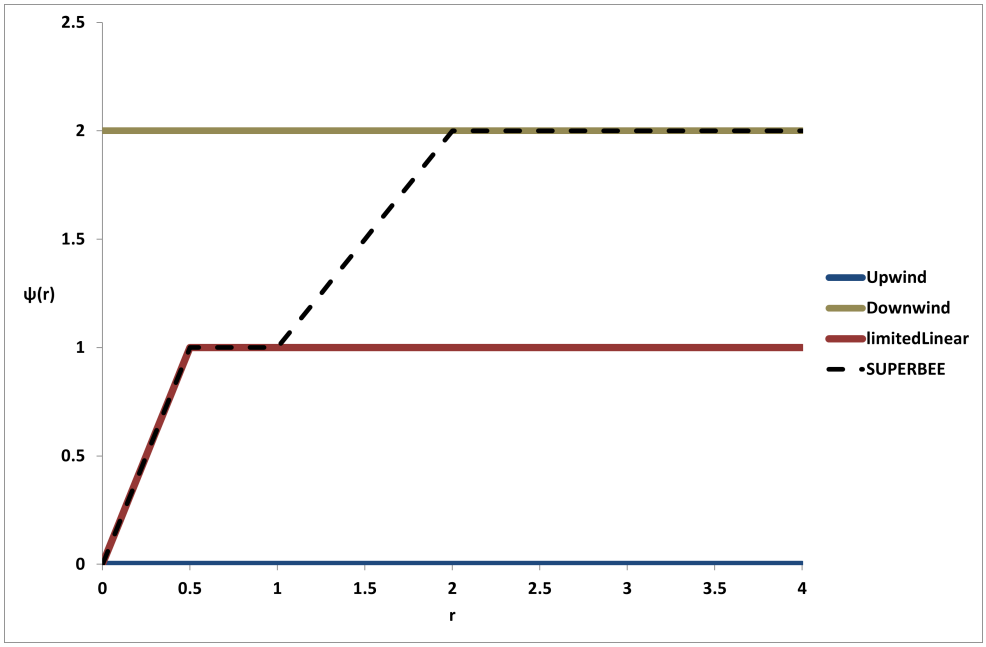

Figure 4. Representation in a Sweby diagram of the "limitedLinear" and "SUPERBEE" limiters.

6. Results

Four simulations have been carried out, three with the original geometry and one with the modified geometry, as shown in Table 1. Except for the simulation with mesh 2, the under-relaxation coefficients are set to 0.3 for the pressure and 0.7 for the velocity. For the simulation on mesh 2, these coefficients are set to 0.9 and 0.5, respectively, for numerical stability reasons during the development of the jet from the initial conditions. For each simulation, the procedure is the same: first, the flow is initialized using an upwind scheme, followed by the use of the "limitedLinear" limiter and, finally, the "SUPERBEE" limiter.

The residuals of the pressure equation are displayed in Figure 5 for the simulations for a stroke of 50%. Whatever the simulation, the pressure residuals are below 2×10^{-5}.

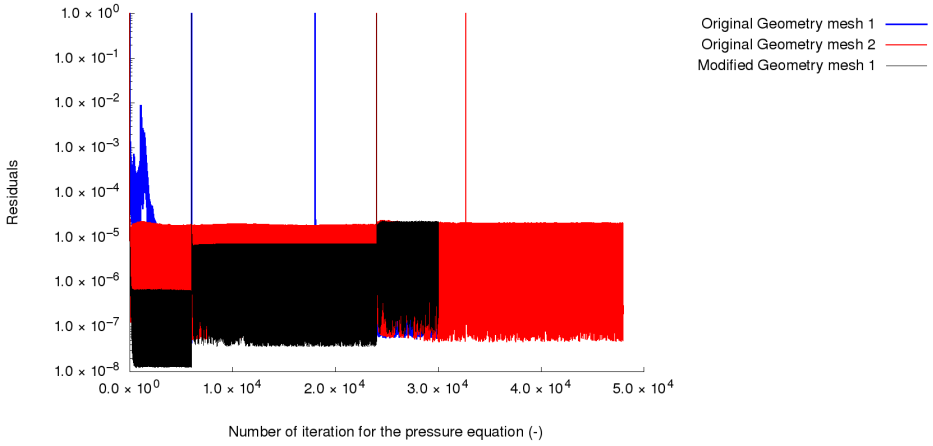

Figure 5. History of the pressure residuals for the three simulations carried out with a stroke of 50%.

The history of the discharge for each simulation is shown in Figure 6 with, in addition, the type of limiter used in different periods. For the original geometry, the type of limiter used influences the discharge predicted by the simulation since by switching to the "SUPERBEE" limiter, the discharge through the nozzle decreases. This is not the case for the modified geometry.

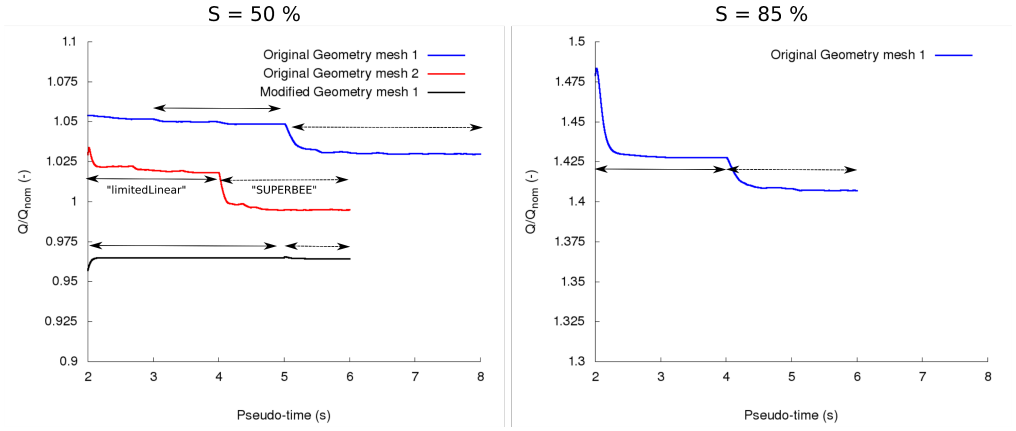

Figure 6. History of the discharge for each simulation. The period over which a specific limiter is used is highlighted by arrows.

In Table 3, the dimensionless discharge (i.e., the discharge divided by the nominal discharge Q_{nom}) predicted by the "limitedLinear" and the "SUPERBEE" limiter are compared for each simulation. Overall, on the original geometry, the simulations with the "limitedLinear" limiter predicts a higher discharge of between 1.4% and 2.3% compared to the simulations with the "SUPERBEE" limiter.

Table 3. Discharge predicted by the simulation depending on the limiter used.

Mesh	Geometry	Stroke (%)	Q/Q_{nom} (−) "limitedLinear"	Q/Q_{nom} (−) "SUPERBEE"	ΔQ (%)
1	Original	50	1.0475	1.03	1.7
2	Original	50	1.0175	0.995	2.3
1	Modified	50	0.965	0.965	0.0
1	Original	85	1.4275	1.4075	1.4

Figures 7–9 compare the iso-surface and the contours of the liquid volume fraction between the different geometries, meshes and limiters used to compute the flow for a needle stroke of 50%. For the modified geometry, the jet is a smooth cylinder, whatever limiter is used (see Figure 7). The jet detaches clearly at the nozzle outlet due to the sharp edge (see Figure 8), and, consequently, the jet is circular downstream (see Figure 9). For the original geometry, the iso-surface is wavy, mainly for mesh 1 (see Figure 7). With mesh 2 and the use of the "SUPERBEE" limiter, the shape of the jet is smoother. These features are also clearly shown in Figure 8 since only the simulation on mesh 2 with the "SUPERBEE" limiter predicts a detachment of the jet at the right location. For the other simulations on the original geometry, the jet is attached to the flat wall of the nozzle. Therefore, downstream of the nozzle outlet, only this simulation predicts a circular jet (see Figure 9), contrary to the other simulations, which predict a non-circular jet with "spikes" at its interface. The use of an anti-diffusive scheme, such as the "SUPERBEE" limiter (and an enough refined mesh), leads to a water/air interface that spreads over a lower number of cell layers than with the "limitedLinear" limiter. Consequently, the jet detaches quickly from the nozzle wall, leading to a more compact jet, which improves the prediction of the jet diameter and the discharge.

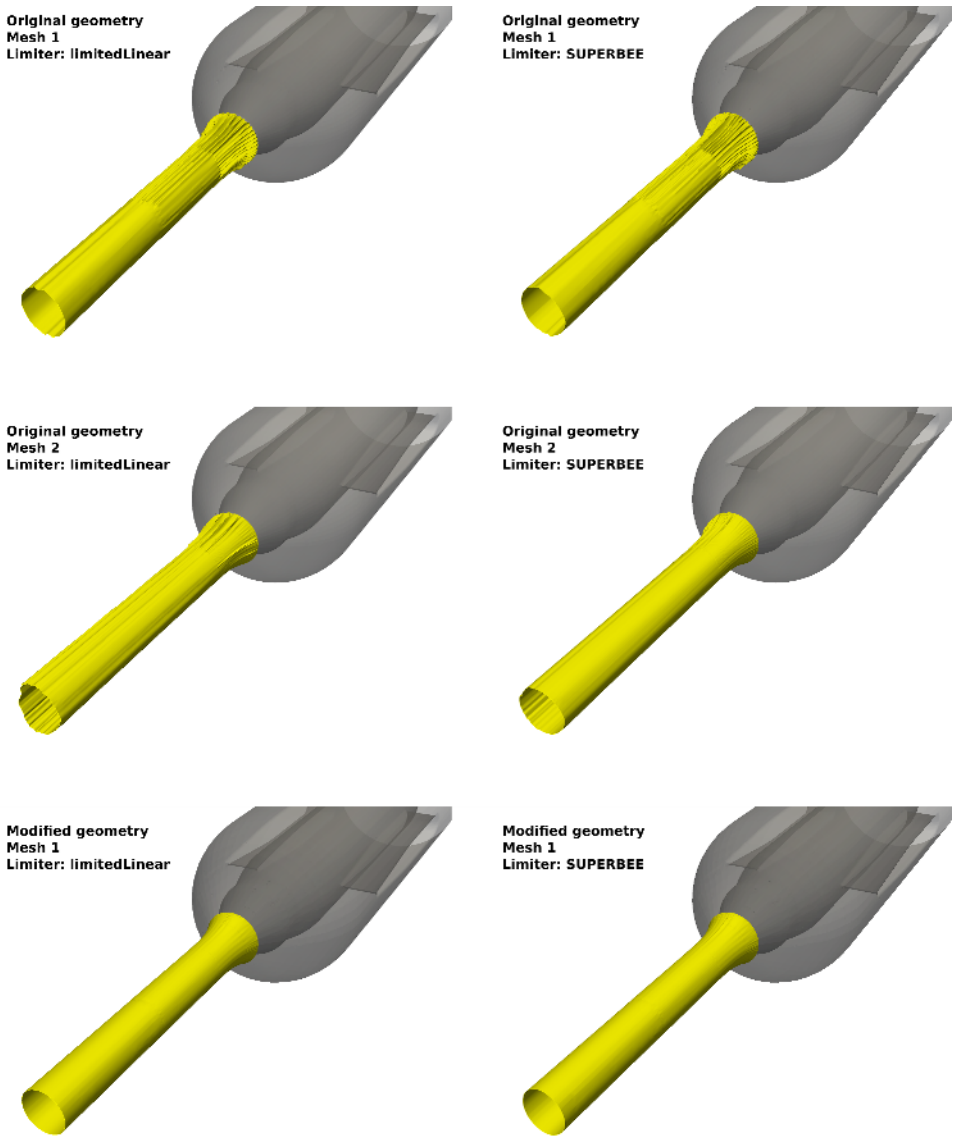

Figure 7. Iso-surface of the liquid volume fraction set to 0.5. Simulations for a needle stroke of 50%.

Figure 10 displays, for a needle stroke of 50% and the simulations with the "SUPERBEE" limiter, the profiles of the liquid volume fraction and the dimensionless axial velocity along the green line shown in Figure 9. The dimensionless radial position r^* is computed as the ratio between the radial position and the nozzle diameter, whereas the dimensionless axial velocity C_a^* is computed as the ratio between the axial velocity and the theoretical jet velocity defined by $\sqrt{2gH}$. The simulation with the original geometry on mesh 2 is characterized by the narrowest jet width, the sharpest interface and the largest velocity deficit (-20%) in the wake of the needle. On mesh 1, the jet width is larger even if the jet interface is sharp and the velocity deficit is weaker, around -10%. The simulation with the modified geometry shows a more diffuse interface since the liquid volume fraction varies from 1 to 0 for half of the jet radius and has a velocity deficit of the same order as the simulation with the original geometry on mesh 1.

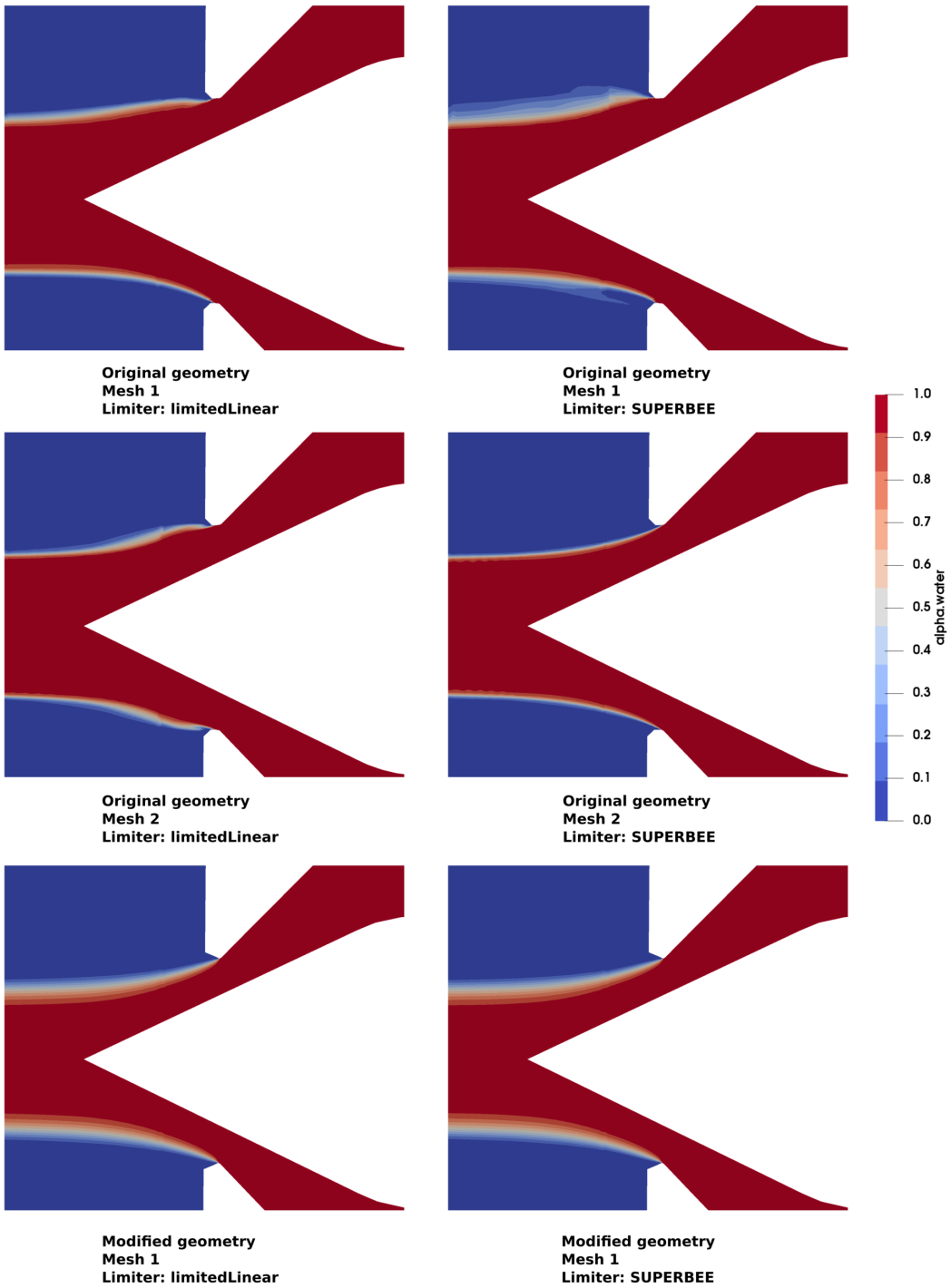

Figure 8. Contour of the liquid volume fraction (*alpha.water*) in the mid-plane aligns with the jet axis. Simulations for a needle stroke of 50%.

On-site measurements allowed a relationship that gives the discharge as a function of the head to be derived [29]. For the nominal head, the dimensionless discharge equals 1 for a stroke of 50% and 1.3675 for a stroke of 80%. Table 4 compares the discharge predicted using the "SUPERBEE" limiter with the on-site measurements. For a stroke of 50%, the simulation using mesh 2 provides better agreement with the on-site measurements with a difference of 0.5%. With mesh 1, the discharge is overestimated by 3.0%, and with the modified geometry, it is underestimated by −3.5%. For a stroke of 85% on mesh 1, the discharge is also overestimated by almost 3% compared to a stroke of 50%.

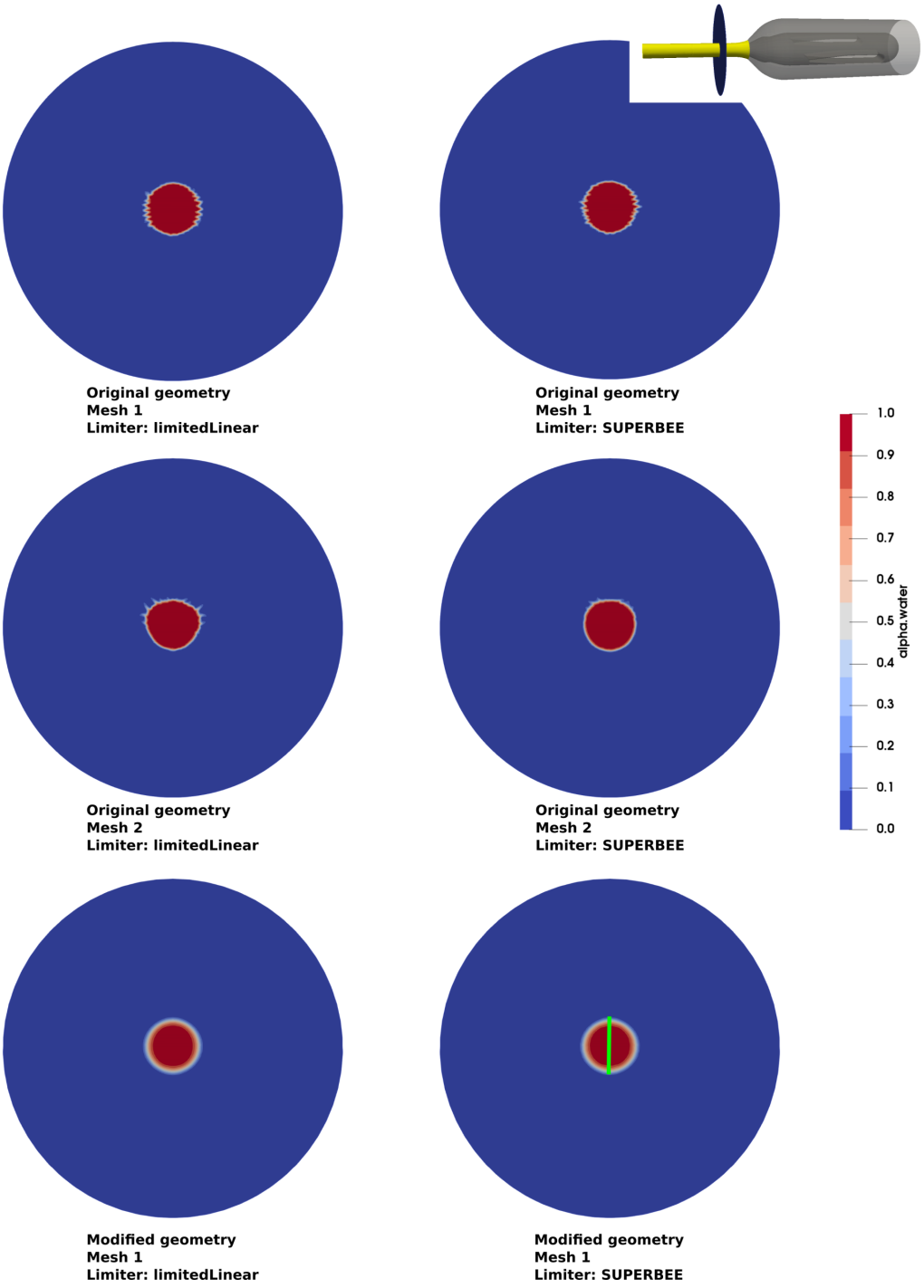

Figure 9. Contour of the liquid volume fraction ($alpha.water$) in a plane perpendicular to jet located at a distance $s = 1.42 \times d_{nozzle}$ downstream the nozzle outlet. Simulations for a needle stroke of 50%. The green line refers to the profiles shown in Figure 10.

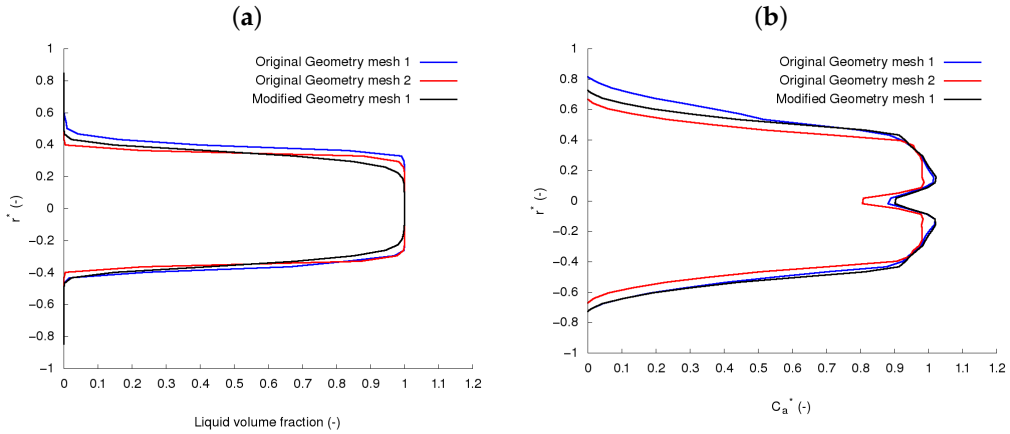

Figure 10. (**a**): Liquid volume fraction profile in the section located at a distance $s = 1.42 \times d_{nozzle}$ downstream of the nozzle outlet. (**b**): Dimensionless axial velocity profile in the section located at a distance $s = 1.42 \times d_{nozzle}$ downstream of the nozzle outlet. The profiles are extracted along the green line shown in Figure 9. Simulations for a needle stroke of 50% with the "SUPERBEE" limiter.

Table 4. Differences between the discharge computed with the SUPERBEE limiter and the measured one.

Mesh Number	Geometry	Stroke (%)	Q/Q_{nom} (−) Computed	Q/Q_{nom} (−) Exp	ΔQ (%)
1	Original	50	1.03		3.0
2	Original	50	0.995	1	−0.5
1	Modified	50	0.965		−3.5
1	Original	85	1.4075	1.3675	2.9

7. Conclusions

Simulations of a Pelton jet with the OpenFOAM toolbox have been performed with a special emphasis on the influence of the nozzle geometry, the mesh and the numerical scheme used for the discretisation of the convective fluxes. The results show the strong influence of the nozzle geometry on the shape of the jet and the discharge predicted by the simulation. By considering a sharp edge at the nozzle outlet, which is not the real geometry, the jet shows a smooth cylindrical shape. In this case, the discharge predicted by the simulation is not influenced by the limiter chosen to discretize the convective fluxes, but it is underestimated by around 3%. On the contrary, by considering the real geometry with a flat section at the nozzle outlet, both the mesh and the limiter have an influence on the jet shape and the discharge predicted. The simulations show that a refined mesh aligned as much as possible with the geometry, as well as the use of an anti-diffusive limiter, such as the "SUPERBEE" limiter, are required to accurately compute the jet detachment, the jet shape and the discharge. Compared to previous studies, the present results show the importance of the numerical schemes used to discretize the convective fluxes. By using an appropriate, low-diffusive scheme such as the "SUPERBEE", "OSHER", or maybe the "UMIST" or "VANLEER" limiter, it is possible to receive accurate results without refining the mesh too much, which allows the saving of time during computation.

The influence of the turbulence model has not been considered in this study because it is not expected to have a strong influence on the jet detachment. On the contrary, an interesting future investigation would be the influence of the surface roughness at the nozzle outlet since this region is subjected to wear and tear.

Author Contributions: Conceptualisation, J.D. and C.M.-A.; methodology, J.D.; software, J.D.; investigation, J.D.; writing—original draft preparation, J.D. and C.M.-A.; project administration, C.M.-A.; funding acquisition, C.M.-A. All authors have read and agreed to the published version of the manuscript.

Funding: This research was funded by SFOE, grant number SI/501636-01, and by FMV (Forces Motrices Valaisannes). The project was carried out in the framework of the Swiss Competence Center for Energy Research for the Supply of Electricity (SCCER-SoE).

Data Availability Statement: The data used for this publication are not publicly available but the authors of the paper can be contacted for discussing the possibility of sharing the data.

Conflicts of Interest: The authors declare no conflict of interest.

Abbreviations

CFD	Compuational Fluid Dynamics
FCT	Flux Transport Corrected
FMHL+	Forces Motrices Hongrin-Léman
FMV	Forces Motrices Valaisannes
KWGO	Kraftwerke Gletsch–Oberwald
MULES	Multidimensional Universal Limiter for Explicit Solution
RANS	Reynolds-Averaged Navier–Stokes
SST	Shear-Stress Transport
TVD	Total Variation Diminishing

References

1. Huertas-Hernando, D.; Farahmand, H.; Holttinen, H.; Kiviluoma, J.; Rinne, E.; Söder, L.; Milligan, M.; Ibanez, E.; Martínez, S.M.; Gomez-Lazaro, E.; et al. Hydro power flexibility for power systems with variable renewable energy sources: An IEA Task 25 collaboration. *Wiley Interdiscip. Rev. Energy Environ.* **2017**, *6*, 1–20. [CrossRef]
2. Nechleba, M. *Hydraulic Turbines: Their Design and Equipment*; Artia: Prague, Czech Republic, 1957.
3. Widmann, W.; Lebesmühlbacher, T.; Ede, A.; Knorpp, K. Design and operation of the Stanzertal hydro power plant headrace tunnel as reservoir. In Proceedings of the Hydro 2015, Harbor, MD, USA, 16–19 March 2015.
4. Münch-Alligné, C.; Decaix, J.; Gaspoz, A.; Hasmatuchi, V.; Dreyer, M.; Nicolet, C.; Alimirzazadeh, S.; Zordan, J.; Manso, P.; Crettenand, S. Production flexibility of small run-of-river power plants: KWGO smart-storage case study. *IOP Conf. Ser. Earth Environ. Sci.* **2021**, *774*, 012037. [CrossRef]
5. Micoulet, G.; Jaccard, A.; Rouge, N. FMHL+: Power extension of the existing Hongrin-Léman powerplant: From the first idea to the first kWh. In Proceedings of the Hydro2016, Montreux, Switzerland, 10–12 October 2016.
6. XFLEX-HYDRO. French Hydropower Plant Aims to Increase Efficiency and Flexibility. XLFEX HYDRO Website. 2022. Available online: https://xflexhydro.net (accessed on 25 May 2022).
7. Pérez-Díaz, J.I.; Sarasúa, J.I.; Wilhelmi, J.R. Contribution of a hydraulic short-circuit pumped-storage power plant to the load–frequency regulation of an isolated power system. *Int. J. Electr. Power Energy Syst.* **2014**, *62*, 199–211. [CrossRef]
8. Sick, M.; Keck, H.; Vullioud, G.; Parkinson, E. New Challenges in Pelton Research. In Proceedings of the Hydro 2000 Conference, Engineers, Australia, 20–23 November 2000.
9. Židonis, A.; Aggidis, G.A. State of the art in numerical modelling of Pelton turbines. *Renew. Sustain. Energy Rev.* **2015**, *45*, 135–144. [CrossRef]
10. Marongiu, J.; Leboeuf, F.; Caro, J.; Parkinson, E. Free surface flows simulations in Pelton turbines using an hybrid SPH-ALE method. *J. Hydraul. Res.* **2009**, *48*, 40–49. [CrossRef]
11. Solemslie, B.W.; Dahlhaug, O.G. A reference Pelton turbine design. *Proc. IOP Conf. Ser. Earth Environ. Sci.* **2012**, *15*, 032005. [CrossRef]
12. Jahanbakhsh, E.; Vessaz, C.; Maertens, A.; Avellan, F. Development of a Finite Volume Particle Method for 3-D fluid flow simulations. *Comput. Methods Appl. Mech. Engrg.* **2016**, *298*, 80–107. [CrossRef]
13. Alimirzazadeh, S.; Kumashiro, T.; Leguizamón, S.; Jahanbakhsh, E.; Maertens, A.; Vessaz, C.; Tani, K.; Avellan, F. GPU-accelerated numerical analysis of jet interference in a six-jet Pelton turbine using Finite Volume Particle Method. *Renew. Energy* **2020**, *148*, 234–246. [CrossRef]
14. Messa, G.V.; Mandelli, S.; Malavasi, S. Hydro-abrasive erosion in Pelton turbine injectors: A numerical study. *Renew. Energy* **2019**, *130*, 474–488. [CrossRef]
15. Tarodiya, R.; Khullar, S.; Levy, A. Assessment of erosive wear performance of Pelton turbine injectors using CFD-DEM simulations. *Powder Technol.* **2022**, *408*, 117763. [CrossRef]
16. Staubli, T.; Abgottspon, A.; Weibel, P.; Bissel, C.; Parkinson, E.; Leduc, J.; Leboeuf, F. Jet quality and Pelton efficiency. In Proceedings of the Hydro 2009, Lyon, France, 26–28 October 2009.
17. Santolin, A.; Cavazzini, G.; Ardizzon, G.; Pavesi, G. Numerical investigation of the interaction between jet and bucket in a Pelton turbine. *Proc. Inst. Mech. Eng. Part A J. Power Energy* **2009**, *223*, 721–728. [CrossRef]

18. Mack, R.; Moser, W. Numerical Investigation of the Flow in a Pelton Turbine. In Proceedings of the XXIst IAHR Symposium on Hydraulic Machinery and Systems, Lausanne, Switzerland, 9–12 September 2002.
19. Jost, D.; Meznar, P.; Lipej, A. Numerical prediction of Pelton turbine efficiency. *IOP Conf. Ser. Earth Environ. Sci.* **2010**, *12*, 012080. [CrossRef]
20. Fiereder, R.; Riemann, S.; Schilling, R. Numerical and experimental investigation of the 3D free surface flow in a model Pelton turbine. *IOP Conf. Ser. Earth Environ. Sci.* **2010**, *12*, 012072. [CrossRef]
21. Barth, T.; Jespersen, D. The design and application of upwind schemes on unstructured meshes. In Proceedings of the 27th Aerospace Sciences Meeting. American Institute of Aeronautics and Astronautics, Reno, NV, USA, 9–12 January 1989. [CrossRef]
22. Brennen, C. *Fundamentals of Multiphase Flow*; Cambridge University Press: Cambridge, UK, 2012.
23. Menter, F.R. Review of the shear-stress transport turbulence model experience from an industrial perspective. *Int. J. Comput. Fluid Dyn.* **2009**, *23*, 305–316. [CrossRef]
24. The OpenFOAM Foundation. Available online: https://openfoam.org/ (accessed on 25 May 2021).
25. Deshpande, S.S.; Anumolu, L.; Trujillo, M.F. Evaluating the performance of the two-phase flow solver interFoam. *Comput. Sci. Discov.* **2012**, *5*, 14016. [CrossRef]
26. Menter, F.R.; Ferreira, J.; Esch, T. The SST Turbulence Model with Improved Wall Treatment for Heat Transfer Predictions in Gas Turbines. In Proceedings of the International Gas Turbine Congress 2003, Tokyo, Japan, 2–7 November 2003; pp. 1–7.
27. Zalesak, S.T. Fully Multidimensional Flux-Corrected Transport Algorithms for Fluids. *J. Comput. Phys.* **1979**, *31*, 335–362. [CrossRef]
28. Moukalled, F.; Mangani, L.; Darwish, M. *The Finite Volume Method in Computational Fluid Dynamics*; Springer: Berlin/Heidelberg, Germany, 2015.
29. Decaix, J.; Gaspoz, A.; Hasmatuchi, V.; Dreyer, M.; Nicolet, C.; Crettenand, S.; Münch-Alligné, C. Enhanced Operational Flexibility of a Small Run-of-River Hydropower Plant. *Water* **2021**, *13*, 1897. [CrossRef]